THE JOURNAL OF PHYSICAL CHEMISTRY B

Article

pubs.acs.org/JPCB

Density Functional Theory Study on the Cross-Linking of Mussel Adhesive Proteins

Mohammad A. Matin,[†] Ramesh Kumar Chitumalla,[†] Manho Lim,[‡] Xingfa Gao,[§] and Joonkyung Jang*[,†]

[†]Department of Nanoenergy Engineering and [‡]Department of Chemistry, Pusan National University, Busan 609-735, Republic of Korea

[§]CAS Key Laboratory for Biomedical Effects of Nanomaterials and Nanosafety, Institute of High Energy Physics, Chinese Academy of Sciences, Beijing 100049, China

Supporting Information

ABSTRACT: The water-resistant adhesion of mussel adhesive proteins (MAPs) to a wet surface requires a cross-linking step, where the catecholic ligands of MAPs coordinate to various transition-metal ions. Fe(III), among the range of metal ions, induces particularly strong cross-linking. The molecular details underlying this cross-linking mediated by transition-metal ions are largely unknown. Of particular interest is the metal−ligand binding energy, which is the molecular origin of the mechanical properties of cross-linked MAPs. Using density functional theory, this study examined the structures and binding energies of various trivalent metal ions (Ti−Ga) forming coordination complexes with a polymeric ligand similar to a MAP. These binding energies were 1 order of magnitude larger than the physisorption energy of a catechol molecule on a metallic surface. On the other hand, the coordination strength of Fe(III) with the ligand was not particularly strong compared to the other metal ions studied. Therefore, the strong cross-linking in the presence of Fe(III) is ascribed to its additional ability as an oxidant to induce covalent cross-linking of the catecholic groups of MAPs.

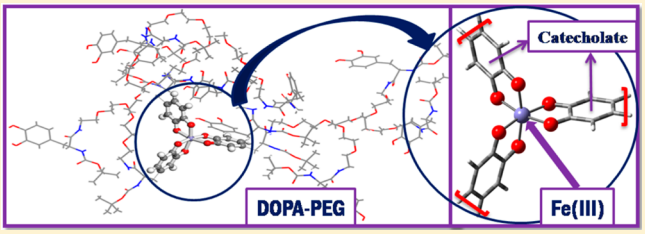

INTRODUCTION

An adhesive sticking irreversibly to wet surfaces has broad applications in areas, such as tissue adhesives, dental cements, and underwater construction.[1] On the other hand, synthesizing a water-resistant adhesive is elusive because the ambient water generally interferes with the adhesion process. Remarkably, marine mussels naturally overcome this obstruction, even under saline and tidal conditions. Thus, far, researchers have found several types of mussel adhesive proteins (MAPs) that can adhere to virtually any surface under wet conditions (e.g., mefp 1−5 for the marine blue mussels).[2−5]

The present understanding of the molecular details underlying the adhesion of MAP is far from complete. The consensus is that the MAPs contain an unusually high content of 3,4-dihydroxy-L-phenylalanine (DOPA). The catechol functionalities (1,2-dihydroxybenzene) of DOPA are believed to play important roles. MAPs adhere to a surface in two stages: initial anchoring on a surface through catechol groups[6−8] and a slow (1−4 h long) curing process in which extensive cross-linking of these MAPs occurs.[9,10] The transition-metal content (e.g., iron, copper, and zinc) in the cross-linking has been reported to reach up to 100 000 times that found in marine water.[1,7,9,11] Therefore, transition-metal ions presumably bring about the cross-linking of MAPs.[9,11,12] Among the many transition-metal ions, the cross-linking of MAPs is quite strong in the presence of Fe(III).[9−11]

Previous studies have revealed two main mechanisms in the cross-linking.[13,14] In the first mechanism, the catechol groups of MAPs are oxidized (to quinones), which are then coupled to form a covalent catechol−catechol linkage.[14,15] In the other mechanism, transition-metal ions, especially Fe(III), coordinate to the dianionic catecholates of MAP to form mono-, bis-, or tris- coordination complexes.[13,16] In contrast to covalent cross-linking, the metal−ligand coordination bonds in the latter mechanism can re-form after breaking. This reversible cross-linking is believed to provide the high elasticity and self-healing properties of cross-linked MAPs.[10,16]

Raman,[10] Fourier transform infrared (FTIR),[7,14,17] ultraviolet−visible (UV−vis), and electron paramagnetic resonance (EPR) spectroscopy partially provide the molecular features of the coordination complexes formed in the cross-linking. The EPR/IR study by Server et al. revealed the presence of the tris-DOPA complexes of Fe(III) in the cross-linked MAPs.[7] The UV−vis spectrum showed the transition from the mono- to bis- and tris- catecholato Fe(III) complexes with increasing pH.[10] Consequently, the gels made of these complexes changed color from green/blue to purple and red. The low-frequency vibrational Raman modes (400−700 cm^{-1}) were attributed to the chelation of the metal ion by the catecholate ligands of

Received: February 4, 2015
Revised: April 1, 2015
Published: April 1, 2015

DOI: 10.1021/acs.jpcb.5b01152
J. Phys. Chem. B 2015, 119, 5496−5504

DOPA.[10,16] The splitting of the FTIR peaks of the DOPA ligand near 1458−1439 cm^{-1} was also attributed to the metal−DOPA coordination.[7] Density functional theory (DFT) calculations of the FTIR and Raman spectra for a tris-DOPA Fe(III) complex concurred with the experimental spectra of a mefp-1 film on an iron substrate.[17]

The present study was particularly interested in the metal−ligand binding energies of the coordination complexes formed in the cross-linking. These binding energies are the molecular origins of the mechanical properties (e.g., shear and compressibility properties) of the cross-linked MAP extracts.[9] This study examined whether the robust cross-linking found in the presence of Fe(III) indeed arises from the strong coordination of Fe(III) to the DOPA ligand. Using DFT, we comparatively studied the structures and stabilities of various transition-metal ions forming coordination compounds with a polymeric ligand imitating a MAP. In particular, the trivalent ions of Ti−Ga developing tris- coordination complexes with a DOPA-modified polyethylene glycol (DOPA-PEG) polymer were considered (Figure 1). This ligand, which was previously

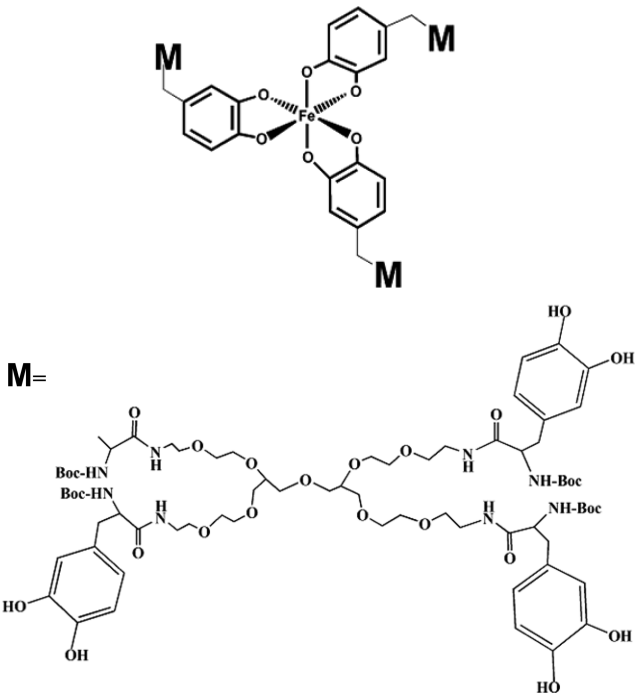

Figure 1. Tris(DOPA-PEG) Fe(III) complex. The bulky part, denoted as M, was treated using the molecular mechanics method, and the rest was modeled using DFT. Boc = butoxycarbonyl ($C(CH_3)_3$−O−CO−).

synthesized to imitate a MAP,[10] was modeled using an ONIOM[18,19] (our own *N*-layer integrated molecular orbital (MO) molecular mechanics (MM)) model. The tris complexes were considered because these are the major forms of the coordination complexes (instead of bis or mono complexes) under a marine environment (pH ≈ 8).[7,10,20] The structures and metal−ligand binding energies of these coordination complexes were examined. Compared to the other metal ions considered, Fe(III) did not show particularly strong binding to the DOPA-PEG ligand. Therefore, the strong cross-linking found for Fe(III) is ascribed to the additional role of Fe(III) as an oxidant to induce the covalent cross-linking of the catecholic groups of MAPs. These conclusions are supported by the Raman, FTIR, and UV−vis spectra, which all agree with the previous spectroscopic data.

COMPUTATIONAL METHODS

We studied the trivalent ions of Ti, V, Cr, Mn, Fe, Co, Ni, Cu, Zn, and Ga forming tris complexes with the DOPA-PEG ligand whose molecular weight (MW) is 1649.9 Da (Figure 1). The catechol group of DOPA was taken to be oxidized (catecholate). The present ONIOM model has two layers. In each coordination complex, the first layer consists of a metal ion and three catecholate groups (37 atoms in total). The first layer was treated by DFT at the level of B3LYP[21]/6-311G(d,p). This hybrid functional has been successfully applied for studying the ferric complexes of catecholic ligands (which are close to the complexes of the present study). For example, the B3LYP DFT simulations of the Raman spectra were in agreement with experimental results.[22,23] The remainder of the complex (denoted by M in Figure 1, made of 657 atoms) was modeled using the MM method employing the universal force field (UFF).[24] Hydrogen was used as the link atom to saturate the dangling bonds of the first layer region.[18] The classical embedding method was used, in which the electrostatic interaction between the partial charges of the two layers was treated classically.[18,25]

As catecholate is a weak-field ligand,[26−28] all of the metal coordination complexes were assumed to have high spin multiplicity. Previous EPR studies also showed that the transition metals form high-spin complexes in their cross-linking with MAPs[7] and with model peptides.[1] We also checked the low-spin and intermediate-spin multiplicities of the Mn, Fe, Co, Ni, and Cu complexes. Except for the Co(III) complex, the high-spin complex of each metal was lower in energy than the low- and intermediate-spin complexes of the same metal. The low-spin complex of Co(III) however was slightly lower, by 0.92 kcal/mol, than that of the high-spin complex (see Table 5).

The present simulations employed the ONIOM scheme[29−35] as implemented in the Gaussian09 simulation package.[36] The two-layer ONIOM method was used,[18] in which the system energy E(ONIOM) is extrapolated as follows

$$E(\text{ONIOM}) = E(\text{real, MM}) + E(\text{model, QM}) - E(\text{model, MM}) \quad (1)$$

The energy of the real system, which includes all of the atoms, E(real, MM), was calculated at the MM level. The energy of the model system, the metal ion, and three catecholates was calculated both at the quantum mechanics (QM) and MM levels to give E(model, QM) and E(model, MM), respectively. We optimized the geometry using the microiterations optimization algorithm.[33] Geometry optimization was taken to be converged if the maximal atomic force was smaller than 0.000015 hartree/Bohr. Unless specified otherwise, no symmetry was imposed in all of the calculations.

After optimizing the geometry of each coordination complex, the metal−ligand binding energy ΔE was calculated as[37]

$$\Delta E = \frac{-(E_{\text{complex}} - E_{\text{metal}} - 3E_{\text{ligand}})}{3} \quad (2)$$

where E_{complex}, E_{metal}, and E_{ligand} are the energies of the tris(DOPA-PEG) coordination complex, the metal ion, and the DOPA-PEG ligand, respectively. Therefore, ΔE refers to the

DOI: 10.1021/acs.jpcb.5b01152
J. Phys. Chem. B 2015, 119, 5496−5504

binding energy per ligand. All of these energies were calculated by optimizing the geometries of the complex and the ligand separately. In the geometry optimization and energy calculation of the DOPA-PEG ligand, the DFT was used at the level of B3LYP/6-311G(d,p). Using the counterpoise correction method,[38] we checked the basis set superposition error (BSSE) for the tris(DOPA-PEG) complexes of trivalent Cr, Mn, Fe, and Co ions (Table S1 of the Supporting Information). The BSSEs were within 7.7% of the binding energies.

The Raman and IR spectra of the tris(DOPA-PEG) Fe(III) complex were calculated by performing frequency calculations using the analytic gradient and Hessian. The raw vibrational frequencies were scaled by a factor of 0.9668, which produced good agreement with the experiment for a wide range of systems.[39]

Electronically excited state calculations were carried out to compute the UV−vis and preresonance Raman spectra of the tris(DOPA-PEG) Fe(III) complex. In these excited-state calculations, the bulky parts were removed, and the dangling bonds were saturated with hydrogen atoms. The geometry however was taken to be the same as that optimized in the presence of the bulky parts. The vertical excitation energies were obtained using the time-dependent DFT[40] at the level of CAM-B3LYP[41]/6-311G(d,p), after the ground-state optimization.

RESULTS AND DISCUSSION

The structural and spectroscopic properties of the tris(DOPA-PEG) Fe(III) complex, which is known to play a central role in many cross-links, were first examined.[9,10,17] Figure 2 shows the

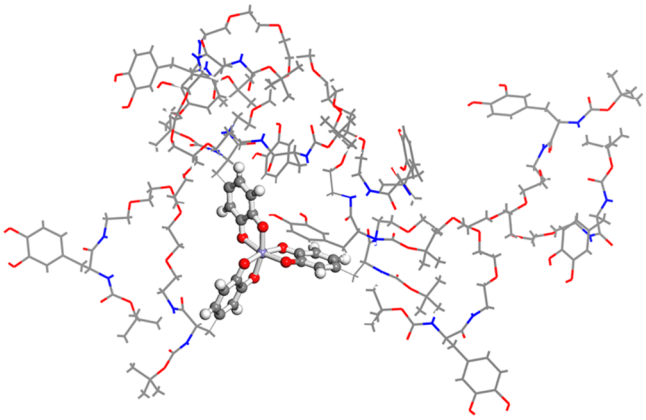

Figure 2. Optimized geometry of the tris(DOPA-PEG) Fe(III) complex. The catecholates of the DOPA-PEG ligand and the metal ion are drawn as balls and sticks, and the rest is drawn as lines.

optimized structure of the tris(DOPA-PEG) Fe(III) complex. The metal and oxygen atoms were 2.06 Å apart on average. The angles formed by the Fe ion and two oxygen atoms of the catecholate ligands were 90.3 (±6.9)° on average, indicating almost octahedral geometry in the coordination. Previous DFT[22] and X-ray analysis[42] of the tris-catecholato Fe(III) complexes reported Fe−O distances of 2.05 and 2.015 Å, respectively. The present O−Fe−O angle was significantly larger than the previous X-ray crystal structure, 81.26°. Another DFT study on a monocatecholato Fe(III) complex[43] reported a Fe−O distance and O−Fe−O angle of 1.933 Å and θ_{OMO} = 86.5°, respectively.

Figure 3 shows the FTIR spectrum of the present tris(DOPA-PEG) Fe(III) complex. Two intense peaks

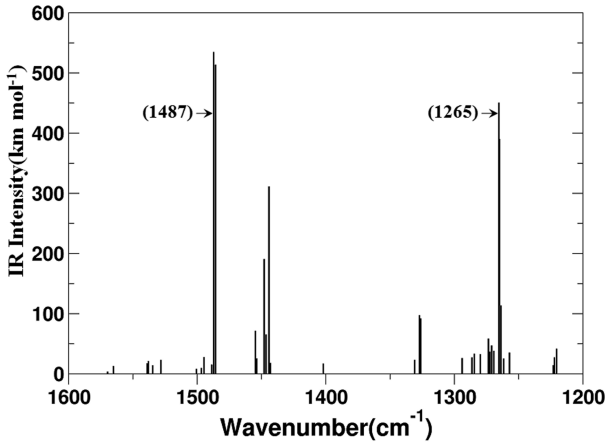

Figure 3. IR spectrum of the tris(DOPA-PEG) Fe(III) complex. The two strongest peaks are indicated by the arrows.

appeared at 1265.03 and 1487 cm^{-1}, along with the two almost degenerate peaks at 1265.43 and 1486 cm^{-1}. Each of these two major peaks originated from an in-plane deformation mode involving the C−C and C−O stretching and the C−H bending of catecholate (see the Supporting Information for arrow plots of the selected IR-active modes). Only two out of three catecholate groups were actively involved in these modes. The mode with a frequency of 1487 cm^{-1} exhibited prominent C−H bending. These two major IR peaks are close in frequency to those previously observed for mefp-1 adsorbed on an iron substrate, 1258 and 1485 cm^{-1}.[17] The high intensities of the present IR peaks arise from the large charge polarization due to the highly positive Fe(III) being surrounded by three negatively charged catecholate ligands. Because of the charge polarization, the vibrations that result in unsymmetrical distortions of the complex induce large dipole moment changes and large IR intensities.

Figure 4 shows the UV−vis absorption spectrum of the tris(DOPA-PEG) Fe(III). Four strong peaks were observed at 488, 489, 513, and 514 nm. The absorption maximum was located at 514 nm, agreeing with the experimental wavelength (492 nm) of the maximal peak found for tris(DOPA-PEG)

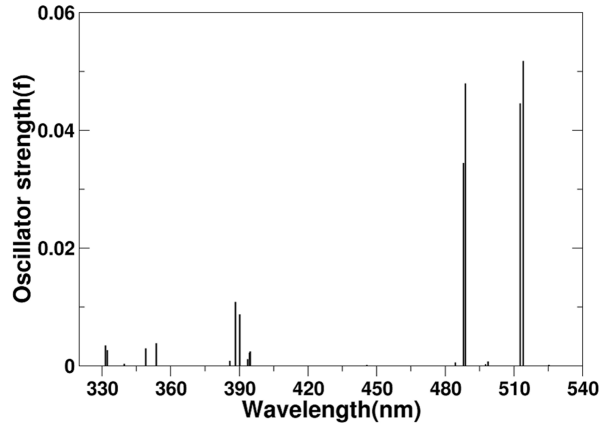

Figure 4. UV−vis spectrum of the tris-catecholato Fe(III) complex obtained from the present calculation.

DOI: 10.1021/acs.jpcb.5b01152
J. Phys. Chem. B 2015, 119, 5496−5504

Fe(III),[10] whose DOPA-PEG ligand (MW = 11 135 kDa) is much longer than the present one (MW = 1.65 kDa). To characterize the electronic transitions, five frontier MOs were illustrated, ranging from the highest occupied MO−2 (HOMO−2) to the lowest unoccupied MO+1 (LUMO+1) (Figure 5). The absorption maximum at 514 nm originated

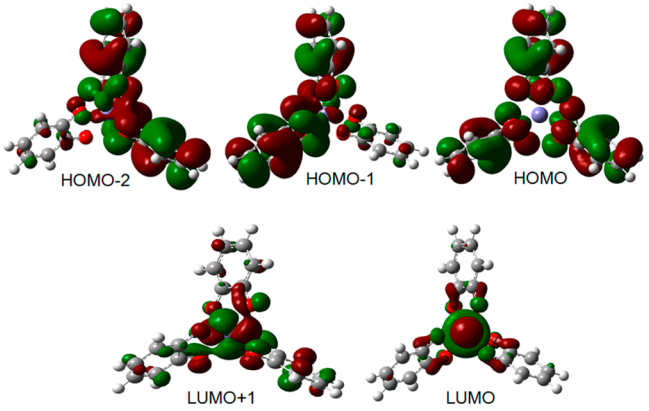

Figure 5. Frontier MOs of the tris-catecholato Fe(III) complex. The H, C, and O atoms are shown as white, gray, and red spheres, respectively. The orbital lobes shown in green and red represent the opposite phases.

predominantly (97%) from the HOMO to LUMO transition. In the HOMO, the electron density is distributed mainly over three catecholate ligands. According to the partial MO composition analysis based the C^2 population analysis[44] (Table 1), only 0.1% of the electron density belongs to the

Table 1. Partial MO Composition (%) of the Present Tris-catecholato Fe(III) Complex[a]

MO	HOMO−2	HOMO−1	HOMO	LUMO	LUMO+1
% Fe	7.1	7.1	0.1	59.5	64.6
energy of MO (eV)	4.56	4.58	4.94	7.63	7.64

[a]The contribution of Fe atomic orbitals to the total MO is shown for five frontier orbitals, ranging from the highest occupied MO−2 (HOMO−2) to the lowest unoccupied MO+1 (LUMO+1).

Fe atomic orbitals (see Table 1). In the LUMO shown in Figure 5, however, the electron density is largely moved out of the catecholates into the Fe ion. The partial MO composition (Table 1) showed that 59.5% of the electron density belongs to the metal ion. Therefore, the strongest peak in the UV−vis spectrum originated clearly from ligand-to-metal charge transfer. The peak at 489 nm primarily (66%) involved the transition from HOMO−2 to LUMO. Again, this peak arose from ligand-to-metal charge transfer; the electron density in HOMO−2 is distributed mostly over two catecholate ligands. The metal ion has only 7.1% of the electron density. The peaks at 488 and 513 nm originated primarily from (70 and 97%, respectively) the HOMO−1 to LUMO and HOMO to LUMO +1 transitions, respectively. The HOMO−1 is similar to the HOMO−2 in that the electron density is spread over two catecholate ligands. The LUMO+1 is similar to the LUMO in that electron density is localized around the metal−oxygen interaction region (64.6% of the electron density belongs to the Fe ion; see Table 1). On the other hand, the LUMO+1 does not have π character of the LUMO orbital.

The vibrational Raman spectrum of the tris-catecholato Fe(III) complex was investigated. Most Raman experiments on the cross-linked MAPs were conducted under the resonance conditions for the electronic transitions. Therefore, the preresonance Raman spectrum was calculated by continuously varying the electronic excitation wavelength from 480 to 560 nm. Using the electronic excitation wavelength of 514 nm, the Raman signal was enhanced up to a factor of 10^{10}, with the Raman peak positions remaining unchanged. The present Raman spectrum, shown in Figure 6, is similar to the Raman spectra measured for mefp-1 films[17] and for the synthetic tris(DOPA-PEG) Fe(III) complex.[10]

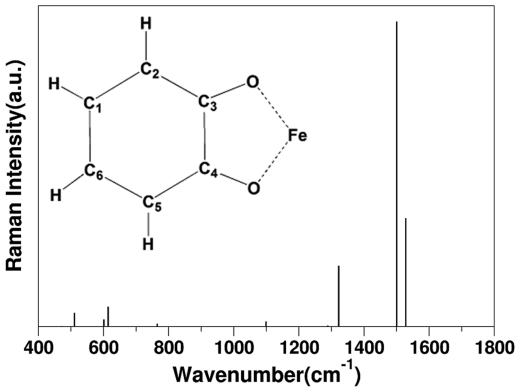

Figure 6. Preresonance Raman spectrum of the tris-catecholato Fe(III) complex calculated using an electronic excitation wavelength of 514 nm.

Table 2 lists the Raman peaks with the nine strongest intensities. The present calculation agrees reasonably with the previous Raman experiments on the synthetic and natural cross-linked MAPs.[10,16,26,45] The low-frequency (512−614 cm^{-1}) modes arose from the chelation of Fe by catecholate. The mode with a frequency of 512 cm^{-1} involved the mixed Fe−O stretching (ν) and O−Fe−O bending (δ) of each catecholate ligand (see the Supporting Information for the arrow plots of the Raman modes listed in Table 2). The Raman mode located at 602 cm^{-1} originated from the Fe−O stretching involving only one of the oxygen atoms of each catecholate. In contrast, the mode at 614 cm^{-1} involved the breathing of all six oxygen atoms surrounding the Fe ion.[10] Previously, similar Fe−O stretching modes were observed in the cross-linking of synthetic polymers[10] and mefp-1.[26]

The Raman peaks with frequencies ≥765 cm^{-1} were assigned to the intramolecular motions of the catecholate ligands. The peak at 765 cm^{-1} was associated with the in-plane C−H bending involving the C2 and C5 atoms of each catecholate ligand (see Figure 6 for carbon indexing). The peak at 1099 cm^{-1} was assigned to another in-plane C−H bending involving C1 and C6 atoms of a single catecholate ligand. The peak at 1288 cm^{-1} consisted of the out-of-phase stretching of two C−O bonds, together with the C−H bending involving C1, C2, C5, and C6 atoms. This mode occurred in two catecholate ligands. The mode at 1322 cm^{-1} was assigned to the in-plane bending of C2−H and C5−H along with C−O stretching, which was found in all three catecholate ligands. The peak at 1500 cm^{-1} arose from C−C stretching mixed with a C−H bending, which occurred in all three catecholate ligands. The peak at 1528 cm^{-1} was assigned to a C−C stretching vibration

DOI: 10.1021/acs.jpcb.5b01152
J. Phys. Chem. B 2015, 119, 5496−5504

Table 2. Pre-resonance Raman Shifts (cm^{-1}) for the Present Tris-catecholato Fe(III) Complex (in bold) along with the Resonance Raman Peaks Previously Measured for the Synthetic and Natural Cross-Linked Structures[a]

A	B	C	D	E	F	G	H	I	J
512	**602**	**614**	**765**	**1099**	**1288**	**1322**		**1500**	**1528**
529[b]	584[b]	634[b]			1270[b]	1324[b]	1422[b]	1484[b]	
533[c]		621[c]	800[c]	1154[c]	1258[c]	1320[c]		1487[c]	1572[c]
531[d]	591[d]	638[d]	815[d]	1152[d]	1274[d]	1326[d]	1426[d]	1491[d]	1571[d]
550[e]	596[e]	637[e]			1270[e]	1322[e]		1423[e]	1476[e]
δ, ν- Fe−O	νFe−O	νFe−O	δC−H	δC−H	νC−O + δC−H	νC−O + δC−H	νC−C[b]	νC−C + δC−H	νC−C + δC−H

[a]The bottom row lists the present assignment of each mode. See Figure 5 for the indexing of the carbon atoms. [b]Synthetic tris(DOPA-PEG) Fe(III) complex formed at pH ≈ 12.[10] [c]Synthetic tris-catecholato Fe(III) complex.[45] [d]Synthetic pink form of MAP cross-linked by forming complexes with Fe(III).[26] [e]Mussel cuticle cross-linked by forming complexes with Fe(III).[16]

plus an in-plane C−H bending vibration involving the C1, C2, C5, and C6 atoms of each catecholate.

The structures of the tris(DOPA-PEG) complexes of various metal ions were then explored comparatively. Table 3 and

Table 3. Geometric Parameters of the Tris(DOPA-PEG) Complexes of Various Metal Ions[a]

metal	d_{MO} (Å)	θ_{OMO} (deg)
Ti	2.09 (±0.01)	90.4 (±8.5)
V	2.05 (±0.04)	90.3 (±7.5)
Cr[b]	2.02 (±0.00)	90.1 (±5.6)
Mn	2.05 (±0.13)	90.1 (±6.3)
Fe	2.06 (±0.00)	90.3 (±7.2)
Co	2.04 (±0.01)	90.3 (±6.9)
Ni	2.08 (±0.02)	90.1 (±6.4)
Cu	2.17 (±0.27)	90.1 (±8.7)
Zn	2.14 (±0.03)	90.2 (±7.9)
Ga	2.04 (±0.01)	90.3 (±6.3)

[a]The metal−O bond lengths (d_{MO}'s) and the O−metal−O bending angles (θ_{OMO}'s) are shown for trivalent metal ions ranging from Ti to Ga(III). The average values are listed with the standard deviations in parentheses. [b]X-ray analysis on a tris-catecholato Cr(III) crystal gave d_{MO} = 1.986 Å and θ_{OMO} = 83.56°.[42]

Figure 7 show the average and standard deviations of the metal−oxygen distances, d_{MO}'s, and the angles of O−metal−O

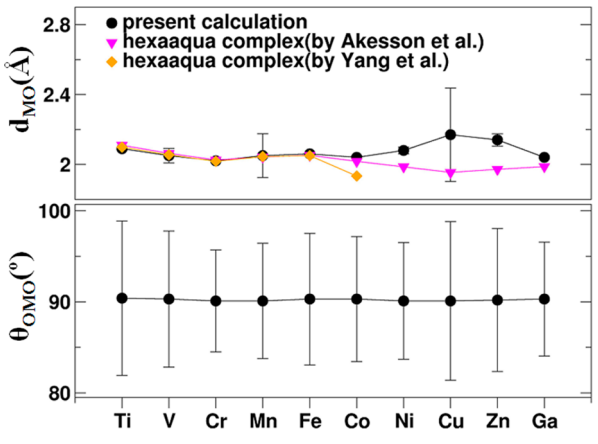

Figure 7. Geometric parameters around the metal ion for the present coordination complexes. The metal−O bond lengths (d_{MO}'s) and the O−metal−O bending angles (θ_{OMO}'s) are plotted. The standard deviations are drawn as error bars. For comparison, the previous calculations of d_{MO}'s for the hexaaqua complexes by Akesson et al.[46] and Yang et al.[47] are plotted. The lines are a guide for the eyes.

triplets, θ_{OMO}'s. The fluctuation in d_{MO} was insignificant (top, Figure 7), except for the Mn and Cu complexes. All the θ_{OMO}'s, however, fluctuate significantly from their average values of approximately 90° (drawn as error bars in the bottom of Figure 7). The present d_{MO}'s are close to those previously calculated for the hexaaqua complexes of the metal ions ranging from Ti to Fe (drawn as diamonds and triangles).[46,47] With increasing nuclear charge, further from Fe, the present d_{MO} increases, reaches a peak at Cu, and then decreases. On the other hand, the d_{MO}'s of the hexaaqua complexes overall decrease with the same change in the nuclear charge. These d_{MO} values, especially for the Cu complex, deviate significantly from those of the hexaaqua complexes.

The atomic charge on the metal ion was checked (Table 4). Five different schemes were used to calculate the charge:

Table 4. Atomic Charges on the Metal Atoms Obtained Using Various Charge Schemes, NPA, MK, CHelpG, CHelp, and HLYGAt

	atomic charge on metal				
metal	NPA	MK	CHelpG	CHelp	HLYGAt
Ti	1.669	1.472	1.730	1.943	1.491
V	1.665	1.434	1.697	1.824	1.434
Cr	1.687	1.354	1.707	1.862	1.460
Mn	1.818	1.400	1.674	1.862	1.463
Fe	1.952	1.448	1.680	1.779	1.489
Co	1.779	1.282	1.564	1.722	1.333
Ni	1.543	1.302	1.458	1.477	1.294
Cu	1.455	1.165	1.340	1.329	1.232
Zn	1.659	1.318	1.498	1.451	1.377
Ga	1.712	1.289	1.590	1.828	1.277

natural population analysis (NPA),[48] MK,[49] CHelpG,[50] and CHelp[51] methods to fit the electrostatic potential, and the charge fitting method, HLYGAt.[52] The atomic charge varied according to the scheme. For example, NPA gave a charge of 1.952 for Fe, but the charge was 1.448 if the MK scheme was used.[49] Overall, the atomic charge decreased with increasing nuclear charge. Nevertheless, the present trend of the atomic charge deviated considerably from a uniform decrease with increasing nuclear charge, as found for the hexaaqua complexes. There, the uniform decrease was attributed to the increased covalent nature of the metal−oxygen bond (hence, the increased charge transfer from the ligand to metal). For the present complexes, however, the atomic charge was a minimum for Cu, regardless of the charge scheme, and the atomic charge sometimes increased with increasing nuclear charge. For example, most charge schemes gave an increasing atomic

DOI: 10.1021/acs.jpcb.5b01152
J. Phys. Chem. B 2015, 119, 5496−5504

charge with the change from Cu to Zn and Ga (except for MK and HLYGAt). The charge also increased as the metal atom was changed from Cr to Mn and Fe, according to the NPA, HLYGAt, and MK schemes.

As shown above, the present ONIOM calculation provides structural and spectroscopic data that are consistent with previous experimental and theoretical work. This study finally investigated the metal−ligand binding energies, ΔE's, of all of the trivalent metal ions considered. Table 5 and Figure 8 show

Table 5. Metal−Ligand Binding Energies of the Present Coordination Complexes[a]

	spin	ΔE (kcal/mol)	ΔE^a (kcal/mol)	ΔE^b (kcal/mol)
Ti	HS	**519.53**	550.50	520.91
V	HS	**549.86**	581.26	540.31
Cr	HS	**555.82**	613.53	553.41
Mn	HS	**552.45**	610.18	542.90
	IS	542.35		
	LS	528.64		
Fe	HS	**540.51**	597.04	540.05
	IS	528.58		
	LS	526.32		
Co	HS	561.95	625.00	569.76
	IS	558.09		
	LS	**562.87**		
Ni	HS	**580.13**	645.79	571.04
	LS	572.79		
Cu	HS	**584.80**	673.76	603.28
	LS	583.49		
Zn	HS	**612.57**	672.56	596.02
Ga	HS	**558.98**	664.44	562.63

[a]The binding energy per ligand ΔE is listed for the tris(DOPA-PEG) complex of each transition metal. The default spin state is taken to be a high spin (HS). The binding energies of the intermediate- and low-spin (IS and LS, respectively) complexes were also calculated. The largest ΔE for a given coordination complex appears in bold. For comparison, the binding energies previously calculated for the hexaaqua complexes, ΔE^a,[46] and the binding energies of the present complexes using the octahedral symmetry ΔE^b,[47] are listed.

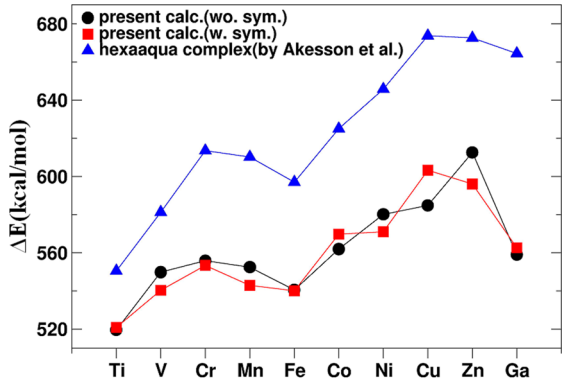

Figure 8. Metal−ligand binding energies of the coordination complexes of various metal ions. The binding energy per ligand ΔE was calculated for each coordination complex without (circles) or with (squares) imposing the octahedral symmetry. For comparison, we show the previous calculation for the hexaaqua complexes. The lines are a guide for the eyes.

that the present ΔE's greatly exceed the typical physisorption energy of a catechol molecule on a metallic surface. Lee et al. reported that a single catechol molecule binds to a titanium surface with a binding energy of 22.2 kcal/mol.[6] A similar energy was reported in a DFT study of the adsorption of DOPA to titanium oxide (25−30 kcal/mol).[53] The present ΔE's are an order of magnitude larger than these. Interestingly, the previous study also reported that Fe(III) coordination produced a 1 order of magnitude increase in the cross-linking strength of DOPA-modified polypeptide amphiphile.[14] The present binding energies (519.53−612.57 kcal/mol) are close to but slightly smaller than those of the hexaaqua complexes (ranging from 550.5 to 673.7 kcal/mol, drawn as triangles in Figure 8).[46]

Figure 8 shows a double-humped feature in the ΔE versus the nuclear charge of metal. Overall, ΔE increases with increasing nuclear charge due to the increased electrostatic interaction with increasing nuclear charge. The decreasing ΔE with changing Cr to Mn arises from the Jahn−Teller distortion of the metal complex.[46] The dip in ΔE observed for Fe was ascribed to the d^5 configuration of Fe(III). In this case, as all of the d orbitals are occupied, the ligand-to-metal charge transfer is inefficient, resulting in a reduced ΔE. This inefficiency also applies to Ga(III), which has a d^{10} configuration. Therefore, ΔE is relatively small for Ga(III). The double-humped features of the ΔE's are similar to those found for the hexaaqua complexes (drawn as triangles in Figure 8).

Note that the presentΔE's have two peaks located at Cr and Zn. The peak at Cr can be understood by noting that the ligand field stabilization should be largest for the d^3 and d^8 configurations of a high-spin complex. The present ΔE reached a maximum for Zn (d^7) but not for Cu (d^8). The difference arises from the fact that the octahedral symmetry was not imposed in this calculation. When the octahedral symmetry was imposed, the resulting ΔE's (drawn as squares, Figure 8) followed exactly the same trend as that found for the hexaaqua complexes, giving the maximal binding energy for Cu.

According to the present ΔE's, Fe(III) is not particularly strong in coordinating to the DOPA-PEG ligand compared to other metal ions considered. Therefore, the strong cross-linking of the MAPs observed in the presence of Fe(III) should derive from other factors. Note that Fe(III) is also capable of oxidizing catechol to quinone, thereby inducing covalent cross-linking of two or more catecholic groups.[9,13,15] Hence, Fe(III) plays double roles of oxidatively inducing the covalent DOPA−DOPA cross-linking and coordinating to the DOPA ligands. Fullenkamp et al. postulated that these dual roles can be switched by an acidic to basic pH change occurring in the course of the byssal secretion and release of mussel adhesion.[13] This study focused on the metal coordination chemistry, but it will be interesting to examine the oxidative covalent cross-linking in the future.

The binding energies above ΔE's included the electronic energies only. The vibrational, thermal, and entropic contributions to ΔE turned out to be small, presumably due to the covalent nature of the metal ligand binding. We calculated the binding energies by including the zero-point energies (ZPEs), thermal energies, enthalpies, and Gibbs free energies (Table S2 of the Supporting Information). Regardless of the metal ion, the ZPE-, thermal-energy-, enthalpy-, Gibbs free energy-corrected ΔE's were all within 6% of the uncorrected binding energies.

We also checked the solvent effects for the Cr, Mn, Fe, and Co complexes by employing the conductor-like polarizable continuum model.[54−56] The energy of each metal complex was

DOI: 10.1021/acs.jpcb.5b01152
J. Phys. Chem. B 2015, 119, 5496−5504

virtually unchanged in a water solvent, only varying by less than 0.003% (Table S3 of the Supporting Information). The structural change of each complex due to the presence of the solvent was not considered in this calculation. We however expect that the near-octahedral geometry around the central metal of each complex remains nearly intact with the introduction of the solvent. Therefore, the present metal−ligand binding energies presumably will not deviate much from those in the solvent. A systematic study on the solvent effects is left as a future work.

CONCLUSION

The underwater adhesion of marine mussels requires mussel adhesive proteins that cross-link to the hardened matrixes on wet surfaces. Transition-metal ions coordinate to the DOPA ligands of the adhesive proteins in the cross-linking. Currently, the molecular structure and binding energy of the metal−DOPA coordination are largely unknown. The metal−DOPA binding energy is one of the molecular origins underlying the mechanical strength of the cross-linked mussel adhesive proteins. In this vein, a DFT study was performed to investigate various transition-metal ions forming tris complexes with a DOPA-modified polymer that mimics a mussel adhesive protein. The present system is similar to the cross-linked structures synthesized and analyzed by Holten-Andersen et al.[10] The present ONIOM calculation simulated the IR, Raman, and UV−vis spectra of the tris(DOPA-PEG) Fe(III) complex, which were all consistent with the previous measurements and calculations. The binding energies of various transition-metal ions coordinating to the DOPA-PEG ligands were calculated. The metal−ligand binding energies were at least 1 order of magnitude larger than that of the metal−surface physisorption. The binding of Fe(III) to the ligand was not particularly strong compared to other metal ions. Therefore, the extra ability of Fe(III) to oxidize the catacholic groups of DOPA and induce the covalent DOPA−DOPA linkage appears to be essential in the strong cross-linking of MAP found in the presence of Fe(III). Future studies will examine the dynamics of the cross-linking, which has not been examined either experimentally or theoretically. The present metal−ligand binding energies, structures, and atomic charges of the metal−DOPA-PEG complexes will serve as a cornerstone for such modeling using molecular dynamics or Monte Carlo simulations.

ASSOCIATED CONTENT

Supporting Information

Table S1: BSSE-corrected binding energies of the selected tris(DOPA-PEG) complexes. Table S2: Metal−ligand binding energies corrected for the ZPEs, thermal energies, enthalpies, and Gibbs free energies. Table S3: Solvent effects on the energies of the tris(DOPA-PEG) complexes of selected metal ions. Full citation of the Gaussian 09 simulation package. Figures of normal modes corresponding to the four major peaks of the IR spectrum. Figures of the normal modes corresponding to the nine strongest peaks of the Raman spectrum. Cartesian coordinates of the tris(DOPA-PEG) Fe(III) used in the calculation of the IR spectrum. Cartesian coordinates of the tris-catecholato Fe(III) complex used in the calculation of the Raman spectrum. This material is available free of charge via the Internet at http://pubs.acs.org.

AUTHOR INFORMATION

Corresponding Author

*E-mail: jkjang@pusan.ac.kr.

Notes

The authors declare no competing financial interest.

ACKNOWLEDGMENTS

This study was supported by the National Research Foundation (NRF) grant funded by the Korean Government (MEST) (No. NRF-2014R1A4A1001690). J.J. acknowledges the support under the framework of international cooperation program managed by the National Research Foundation of Korea (No. 2014-K2A2A2000610).

REFERENCES

(1) Weisser, J. T.; Nilges, M. J.; Sever, M. J.; Wilker, J. J. Epr Investigation and Spectral Simulations of Iron−Catecholate Complexes and Iron−Peptide Models of Marine Adhesive Cross-Links. *Inorg. Chem.* **2006**, *45*, 7736−7747.

(2) Waite, J. H.; Qin, X. Polyphosphoprotein from the Adhesive Pads of *Mytilus edulis*. *Biochemistry* **2001**, *40*, 2887−2893.

(3) Mian, S. A.; Saha, L. C.; Jang, J.; Wang, L.; Gao, X.; Nagase, S. Density Functional Theory Study of Catechol Adhesion on Silica Surfaces. *J. Phys. Chem. C* **2010**, *114*, 20793−20800.

(4) Mian, S.; Gao, X.; Nagase, S.; Jang, J. Adsorption of Catechol on a Wet Silica Surface: Density Functional Theory Study. *Theor. Chem. Acc.* **2011**, *130*, 333−339.

(5) Deming, T. J. Mussel Byssus and Biomolecular Materials. *Curr. Opin. Chem. Biol.* **1999**, *3*, 100−105.

(6) Lee, H.; Scherer, N. F.; Messersmith, P. B. Single-Molecule Mechanics of Mussel Adhesion. *Proc. Natl. Acad. Sci. U.S.A.* **2006**, *103*, 12999−13003.

(7) Sever, M. J.; Weisser, J. T.; Monahan, J.; Srinivasan, S.; Wilker, J. J. Metal-Mediated Cross-Linking in the Generation of a Marine-Mussel Adhesive. *Angew. Chem., Int. Ed.* **2004**, *43*, 448−450.

(8) Avdeef, A.; Sofen, S. R.; Bregante, T. L.; Raymond, K. N. Coordination Chemistry of Microbial Iron Transport Compounds. 9. Stability Constants for Catechol Models of Enterobactin. *J. Am. Chem. Soc.* **1978**, *100*, 5362−5370.

(9) Monahan, J.; Wilker, J. J. Specificity of Metal Ion Cross-Linking in Marine Mussel Adhesives. *Chem. Commun.* **2003**, 1672−1673.

(10) Holten-Andersen, N.; Harrington, M. J.; Birkedal, H.; Lee, B. P.; Messersmith, P. B.; Lee, K. Y. C.; Waite, J. H. pH-Induced Metal−Ligand Cross-Links Inspired by Mussel Yield Self-Healing Polymer Networks with near-Covalent Elastic Moduli. *Proc. Natl. Acad. Sci. U.S.A.* **2011**, *108*, 2651−2655.

(11) Monahan, J.; Wilker, J. J. Cross-Linking the Protein Precursor of Marine Mussel Adhesives: Bulk Measurements and Reagents for Curing. *Langmuir* **2004**, *20*, 3724−3729.

(12) Taylor, S. W.; Waite, J. H.; Ross, M. M.; Shabanowitz, J.; Hunt, D. F. *trans*-2,3-*cis*-3,4-Dihydroxyproline, a New Naturally Occurring Amino Acid, Is the Sixth Residue in the Tandemly Repeated Consensus Decapeptides of an Adhesive Protein from Mytilus Edulis. *J. Am. Chem. Soc.* **1994**, *116*, 10803−10804.

(13) Fullenkamp, D. E.; Barrett, D. G.; Miller, D. R.; Kurutz, J. W.; Messersmith, P. B. pH-Dependent Cross-Linking of Catechols through Oxidation via Fe^{3+} and Potential Implications for Mussel Adhesion. *RSC Adv.* **2014**, *4*, 25127−25134.

(14) Ceylan, H.; Urel, M.; Erkal, T. S.; Tekinay, A. B.; Dana, A.; Guler, M. O. Mussel Inspired Dynamic Cross-Linking of Self-Healing Peptide Nanofiber Network. *Adv. Funct. Mater.* **2013**, *23*, 2081−2090.

(15) Barrett, D. G.; Fullenkamp, D. E.; He, L.; Holten-Andersen, N.; Lee, K. Y. C.; Messersmith, P. B. pH-Based Regulation of Hydrogel Mechanical Properties through Mussel-Inspired Chemistry and Processing. *Adv. Funct. Mater.* **2013**, *23*, 1111−1119.

DOI: 10.1021/acs.jpcb.5b01152
J. Phys. Chem. B 2015, 119, 5496−5504

(16) Harrington, M. J.; Masic, A.; Holten-Andersen, N.; Waite, J. H.; Fratzl, P. Iron-Clad Fibers: A Metal-Based Biological Strategy for Hard Flexible Coatings. *Science* **2010**, *328*, 216−220.
(17) Zhang, F.; Sababi, M.; Brinck, T.; Persson, D.; Pan, J.; Claesson, P. M. In Situ Investigations of Fe^{3+} Induced Complexation of Adsorbed Mefp-1 Protein Film on Iron Substrate. *J. Colloid Interface Sci.* **2013**, *404*, 62−71.
(18) Vreven, T.; Byun, K. S.; Komáromi, I.; Dapprich, S.; Montgomery, J. A.; Morokuma, K.; Frisch, M. J. Combining Quantum Mechanics Methods with Molecular Mechanics Methods in ONIOM. *J. Chem. Theory Comput.* **2006**, *2*, 815−826.
(19) Singh, U. C.; Kollman, P. A. A Combined Ab Initio Quantum Mechanical and Molecular Mechanical Method for Carrying out Simulations on Complex Molecular Systems: Applications to the $CH_3Cl + Cl^-$ Exchange Reaction and Gas Phase Protonation of Polyethers. *J. Comput. Chem.* **1986**, *7*, 718−730.
(20) Zeng, H.; Hwang, D. S.; Israelachvili, J. N.; Waite, J. H. Strong Reversible Fe^{3+}-Mediated Bridging between DOPA-Containing Protein Films in Water. *Proc. Natl. Acad. Sci. U.S.A.* **2010**, *107*, 12850−12853.
(21) Becke, A. D. Density-Functional Thermochemistry. III. The Role of Exact Exchange. *J. Chem. Phys.* **1993**, *98*, 5648−5652.
(22) Horsman, G. P.; Jirasek, A.; Vaillancourt, F. H.; Barbosa, C. J.; Jarzecki, A. A.; Xu, C.; Mekmouche, Y.; Spiro, T. G.; Lipscomb, J. D.; Blades, M. W.; et al. Spectroscopic Studies of the Anaerobic Enzyme−Substrate Complex of Catechol 1,2-Dioxygenase. *J. Am. Chem. Soc.* **2005**, *127*, 16882−16891.
(23) Šebestík, J.; Šafařík, M.; Bouř, P. Ferric Complexes of 3-Hydroxy-4-Pyridinones Characterized by Density Functional Theory and Raman and Uv−Vis Spectroscopies. *Inorg. Chem.* **2012**, *51*, 4473−4481.
(24) Rappe, A. K.; Casewit, C. J.; Colwell, K. S.; Goddard, W. A.; Skiff, W. M. UFF, a Full Periodic Table Force Field for Molecular Mechanics and Molecular Dynamics Simulations. *J. Am. Chem. Soc.* **1992**, *114*, 10024−10035.
(25) Bakowies, D.; Thiel, W. Hybrid Models for Combined Quantum Mechanical and Molecular Mechanical Approaches. *J. Phys. Chem.* **1996**, *100*, 10580−10594.
(26) Taylor, S. W.; Chase, D. B.; Emptage, M. H.; Nelson, M. J.; Waite, J. H. Ferric Ion Complexes of a DOPA-Containing Adhesive Protein from Mytilus Edulis. *Inorg. Chem.* **1996**, *35*, 7572−7577.
(27) Yapo-Kicho, D.; Lagant, P.; Vergoten, G. The SPASIBA Force Field for Studying Iron−Tannins Interactions: Application to Fe^{3+}/Fe^{2+} Catechol Complexe. *Int. J. Mol. Sci.* **2007**, *8*, 259−272.
(28) Cox, D. D.; Que, L. Functional Models for Catechol 1,2-Dioxygenase. The Role of the Iron(III) Center. *J. Am. Chem. Soc.* **1988**, *110*, 8085−8092.
(29) Karadakov, P. B.; Morokuma, K. ONIOM as an Efficient Tool for Calculating NMR Chemical Shielding Constants in Large Molecules. *Chem. Phys. Lett.* **2000**, *317*, 589−596.
(30) Rega, N.; Iyengar, S. S.; Voth, G. A.; Schlegel, H. B.; Vreven, T.; Frisch, M. J. Hybrid Ab-Initio/Empirical Molecular Dynamics: Combining the ONIOM Scheme with the Atom-Centered Density Matrix Propagation (ADMP) Approach. *J. Phys. Chem. B* **2004**, *108*, 4210−4220.
(31) Humbel, S.; Sieber, S.; Morokuma, K. The IMOMO Method: Integration of Different Levels of Molecular Orbital Approximations for Geometry Optimization of Large Systems: Test for *n*-Butane Conformation and S_N2 Reaction: $RCl+Cl^-$. *J. Chem. Phys.* **1996**, *105*, 1959−1967.
(32) Vreven, T.; Morokuma, K. Investigation of the S0−S1 Excitation in Bacteriorhodopsin with the Oniom(MO:MM) Hybrid Method. *Theor. Chem. Acc.* **2003**, *109*, 125−132.
(33) Vreven, T.; Morokuma, K. On the Application of the IMOMO (Integrated Molecular Orbital + Molecular Orbital) Method. *J. Comput. Chem.* **2000**, *21*, 1419−1432.
(34) Derat, E.; Bouquant, J.; Humbel, S. On the Link Atom Distance in the ONIOM Scheme. An Harmonic Approximation Analysis. *J. Mol. Struct.: THEOCHEM* **2003**, *632*, 61−69.
(35) Théry, V.; Rinaldi, D.; Rivail, J.-L.; Maigret, B.; Ferenczy, G. G. Quantum Mechanical Computations on Very Large Molecular Systems: The Local Self-Consistent Field Method. *J. Comput. Chem.* **1994**, *15*, 269−282.
(36) Frisch, M. J. T, G. W.; Schlegel, H. B.; Scuseria, G. E.; Robb, M. A.; Cheeseman, J. R.; Scalmani, G.; Barone, V.; Mennucci, B.; Petersson, G. A.; et al. *Gaussian 09*, revision B.01; Gaussian, Inc.: Wallingford, CT, 2010.
(37) Myradalyyev, S.; Limpanuparb, T.; Wang, X.; Hirao, H. Comparative Computational Analysis of Binding Energies between Several Divalent First-Row Transition Metals (Cr^{2+}, Mn^{2+}, Fe^{2+}, Co^{2+}, Ni^{2+}, and Cu^{2+}) and Ligands (Porphine, Corrin, and Tmc). *Polyhedron* **2013**, *52*, 96−101.
(38) Boys, S. F.; Bernardi, F. The Calculation of Small Molecular Interactions by the Differences of Separate Total Energies. Some Procedures with Reduced Errors. *Mol. Phys.* **1970**, *19*, 553−566.
(39) Merrick, J. P.; Moran, D.; Radom, L. An Evaluation of Harmonic Vibrational Frequency Scale Factors. *J. Phys. Chem. A* **2007**, *111*, 11683−11700.
(40) Furche, F.; Burke, K. In *Annual Reports in Computational Chemistry*; David, C. S., Ed.; Elsevier: New York, 2005; Vol. *1*, pp 19−30.
(41) Yanai, T.; Tew, D. P.; Handy, N. C. A New Hybrid Exchange−Correlation Functional Using the Coulomb-Attenuating Method (CAM-B3LYP). *Chem. Phys. Lett.* **2004**, *393*, 51−57.
(42) Raymond, K. N.; Isied, S. S.; Brown, L. D.; Fronczek, F. R.; Nibert, J. H. Coordination Isomers of Biological Iron Transport Compounds. VI. Models of the Enterobactin Coordination Site. A Crystal Field Effect in the Structure of Potassium Tris(catecholato)-chromate(III) and -Ferrate(III) Sesquihydrates, $K_3[M(O_2C_6H_4)_3]\cdot 1.5H_2O$, M = Chromium, Iron. *J. Am. Chem. Soc.* **1976**, *98*, 1767−1774.
(43) Öhrström, L.; Michaud-Soret, I. Fe−Catecholate and Fe−Oxalate Vibrations and Isotopic Substitution Shifts from Dft Quantum Chemistry. *J. Phys. Chem. A* **1999**, *103*, 256−264.
(44) Ros, P.; Schuit, G. C. A. Molecular Orbital Calculations on Copper Chloride Complexes. *Theor. Chim. Acta* **1966**, *4*, 1−12.
(45) Salama, S.; Stong, J. D.; Neilands, J. B.; Spiro, T. G. Electronic and Resonance Raman Spectra of Iron(III) Complexes of Enterobactin, Catechol, and *N*-Methyl-2,3-dihydroxybenzamide. *Biochemistry* **1978**, *17*, 3781−3785.
(46) Aakesson, R.; Pettersson, L. G. M.; Sandstroem, M.; Wahlgren, U. Ligand Field Effects in the Hydrated Divalent and Trivalent Metal Ions of the First and Second Transition Periods. *J. Am. Chem. Soc.* **1994**, *116*, 8691−8704.
(47) Yang, Y.; Ratner, M. A.; Schatz, G. C. Multireference Ab Initio Study of Ligand Field D−D Transitions in Octahedral Transition-Metal Oxide Clusters. *J. Phys. Chem. C* **2014**, *118*, 29196−29208.
(48) Reed, A. E.; Weinstock, R. B.; Weinhold, F. Natural Population Analysis. *J. Chem. Phys.* **1985**, *83*, 735−746.
(49) Singh, U. C.; Kollman, P. A. An Approach to Computing Electrostatic Charges for Molecules. *J. Comput. Chem.* **1984**, *5*, 129−145.
(50) Breneman, C. M.; Wiberg, K. B. Determining Atom-Centered Monopoles from Molecular Electrostatic Potentials. The Need for High Sampling Density in Formamide Conformational Analysis. *J. Comput. Chem.* **1990**, *11*, 361−373.
(51) Chirlian, L. E.; Francl, M. M. Atomic Charges Derived from Electrostatic Potentials: A Detailed Study. *J. Comput. Chem.* **1987**, *8*, 894−905.
(52) Hu, H.; Lu, Z.; Yang, W. Fitting Molecular Electrostatic Potentials from Quantum Mechanical Calculations. *J. Chem. Theory Comput.* **2007**, *3*, 1004−1013.
(53) Vega-Arroyo, M.; LeBreton, P. R.; Rajh, T.; Zapol, P.; Curtiss, L. A. Density Functional Study of the TiO_2−Dopamine Complex. *Chem. Phys. Lett.* **2005**, *406*, 306−311.
(54) Barone, V.; Cossi, M. Quantum Calculation of Molecular Energies and Energy Gradients in Solution by a Conductor Solvent Model. *J. Phys. Chem. A* **1998**, *102*, 1995−2001.

DOI: 10.1021/acs.jpcb.5b01152
J. Phys. Chem. B 2015, 119, 5496−5504

(55) Cossi, M.; Rega, N.; Scalmani, G.; Barone, V. Energies, Structures, and Electronic Properties of Molecules in Solution with the C-PCM Solvation Model. *J. Comput. Chem.* **2003**, *24*, 669−681.
(56) Tomasi, J.; Mennucci, B.; Cammi, R. Quantum Mechanical Continuum Solvation Models. *Chem. Rev.* **2005**, *105*, 2999−3094.

DOI: 10.1021/acs.jpcb.5b01152
J. Phys. Chem. B 2015, 119, 5496−5504